Ethynylene-analogues of hemicurcuminoids: Synthesis and ground- and excited properties of their boron difluoride complexes

B. Štefane, F. Požgan, E. Kim, E. Choi, J.-C. Ribierre, J.W. Wu, Miguel-Armando Ponce-Vargas, Boris Le Guennic, D. Jacquemin, Gabriel Canard, et al.

Excitation (Visible light)

Fluorescence

Ethynylene-Analogues of Hemicurcuminoids: Synthesis and Ground- and Excited Properties of their Boron Difluoride Complexes

Bogdan Štefane,[a,*] Franc Požgan,[a] Eunsun Kim,[b] Eunyoung Choi,[b] Jean-Charles Ribierre,[b] Jeong Weon Wu,[b] Miguel Ponce-Vargas,[c] Boris Le Guennic,[c,*] Denis Jacquemin,[d,e] Gabriel Canard,[f] Elena Zaborova,[f] Frédéric Fages,[f,*] Anthony D'Aléo[b,f,*]

[a] Faculty of Chemistry and Chemical Technology, University of Ljubljana, Večna pot 113, SI-1000 Ljubljana, Slovenia, bogdan.stefane@fkkt.uni-lj.si.

[b] Department of Physics, Quantum MetaMaterials Research Center, Ewha Womans University, Seoul, Korea.

[c] Institut des Sciences Chimiques de Rennes, UMR 6226 CNRS-Université de Rennes 1, 263 Avenue du Général Leclerc, 35042 Rennes Cedex, France, boris.leguennic@univ-rennes1.fr.

[d] Laboratoire CEISAM, UMR CNRS 6230, Université de Nantes, 2 Rue de la Houssinière, BP 92208, 44322 Nantes Cedex 3, France.

[e] Institut Universitaire de France, rue Descartes, 75231 Paris Cedex 05, France

[f] Aix Marseille Univ, CNRS, CINaM UMR 7325, Campus de Luminy, Case 913, 13288 Marseille, France, frederic.fages@univ-amu.fr, daleo@cinam.univ-mrs.fr.

Abstract:

The synthesis, characterization and (TD)-DFT calculations of the electrochemical and photophysical properties of novel ethynylene-analogues of hemicurcuminoids are described. These dyes are both emissive in solution and in the solid state. While compounds that emit through an efficient charge transfer (CT) state show solvatochromic behavior associated with low fluorescence quantum yields, those lacking of donor groups show high fluorescence quantum yields of 70-80%, in solution. The latter dyes also present the advantage to emit in the solid state in the visible region with fluorescence quantum yields up to 23%. Their condensed phase spectrum can be bathochromically shifted to the near infrared region (742 nm) by appending a strong donor group.

1. Introduction

The design and synthesis of novel fluorescent dyes with tailored properties is a constantly growing field of research due to exciting applications in bio-imaging [1-3] and emitting devices.[4-8] In those applications, the selection of the best dyes requires to optimize several parameters such as absorption and emission wavelengths, molar absorption coefficients, fluorescence quantum yields, and Stokes shifts.

Molecules containing the boron difluoride (BF$_2$) moiety, such as the well-known BODIPYs[9-12] and aza-BODIPYs[13-15] represent one of the most important family of fluorophores that have been exploited in many different kinds of applications, as they present very large fluorescence quantum yields in solution. However, similarly to cyanine dyes, most (aza)-BODIPY dyes show a small Stokes shift and do not exhibit luminescence in their solid state unless they feature bulky groups[16] or aggregation induced emission properties.[17, 18] In this context, we and others developed series of boron difluoride complexes of acetylacetone-like chelate,[19-27] curcuminoid[28-32] and hemicurcuminoid[33, 34] derivatives with the aim to combine the electron withdrawing BF$_2$ moiety to electron donor groups. As such systems develop a push-pull character, this should allow overcoming the Stokes shift issue as well as the quenching of the fluorescence in the condensed phase. Indeed, BF$_2$ complexes of curcuminoids and hemicurcuminoids proved to be versatile fluorophores allowing the preparation of fluorescent organic nanoparticles useful for bio-imaging purposes relying on both one- and two-photon excitation techniques.[31, 34, 35]
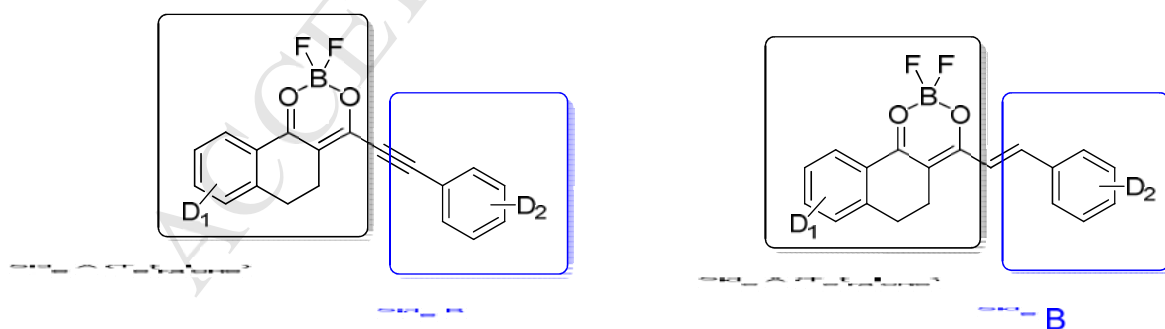
Scheme 1. Structures of the hemicurcuminoid derivatives (right) and the new ethynylene analogues (left) investigated in this study (where D$_1$ and D$_2$ are the donor groups).

We report herein the synthesis and electrochemical and optical properties in both solution and solid state of an unprecedented related series of BF_2-containing hemicurcuminoids in which the dioxaborine-containing subunit (side A) and the terminal aromatic group (side B) are connected *via* an acetylenic linkage (Scheme 1).[34] More specifically, side A consists in the BF_2 complex of a tetralone-containing acetylacetone moiety and side B features various donor groups. We were interested in investigating the influence of the ethynylene spacer on the excited states properties in solution and fluorescence emission characteristics in the solid state and compare the properties to the corresponding vinylene compounds.[34] Density Functional Theory (DFT) and Time-Dependent Density Functional Theory (TD-DFT) calculations were performed in order to provide insights into the factors that control the optical and electrochemical properties of the hemicurcuminoid-related dyes.

1: R_1= H, R_2= H
2: R_1= H, R_2= MeO
3: R_1= Cl, R_2= MeO
4: R_1= MeO, R_2= H
5: R_1= Me$_2$N, R_2= H

6

7

M'1: R_1= H
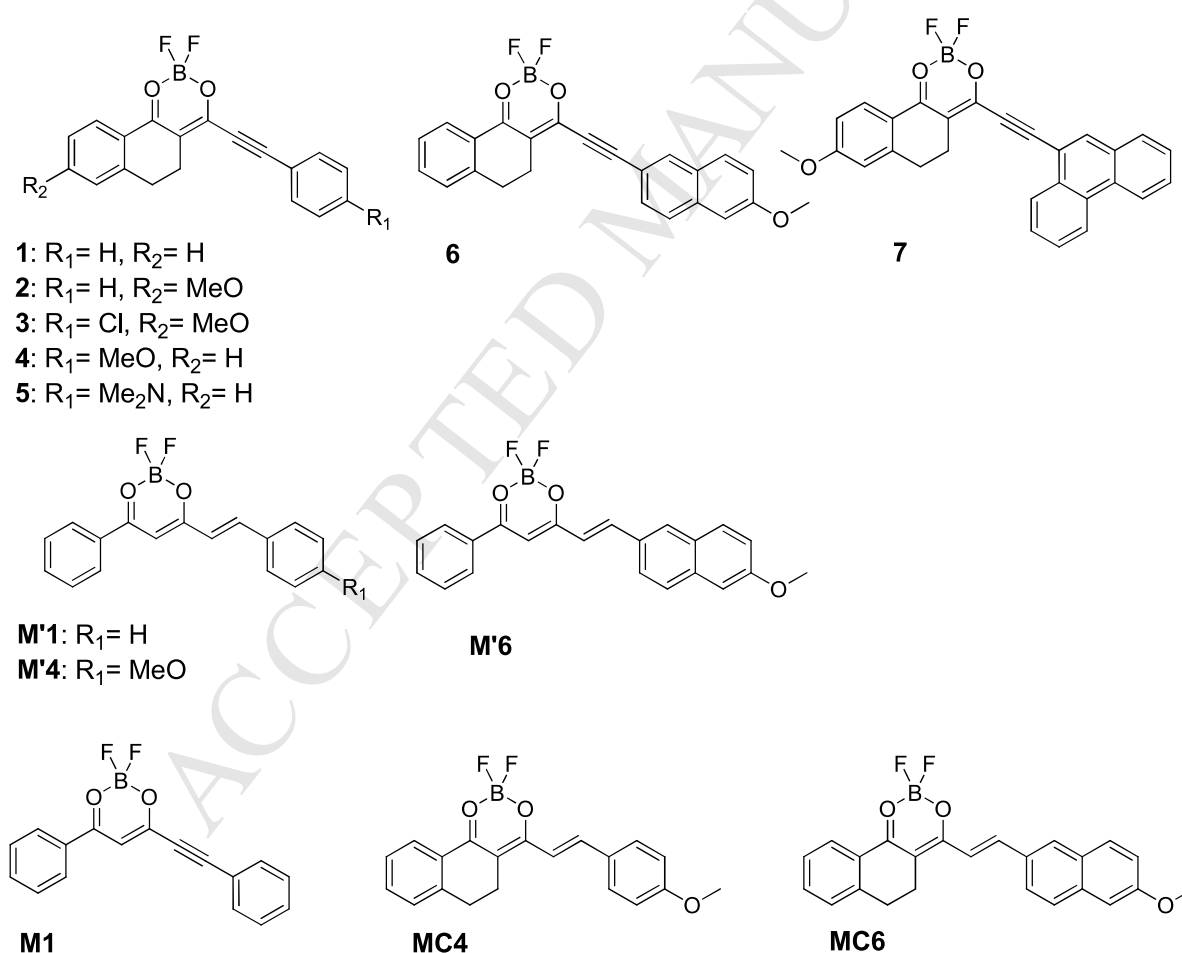**M'4**: R_1= MeO

M'6

M1

MC4

MC6

Chart 1. Structures of the boron difluoride dyes investigated and discussed herein.

2. Experimental

Materials and Instrumentation. All solvents for synthesis were of analytic grade. Spectroscopy measurements were carried out with spectroscopic grade solvents. The complexes **1**,[36] **M1**,[36] **M'1**,[34] **M'4**[34] and **M'6**[34] were previously. NMR spectra (^{1}H, ^{13}C, ^{19}F) were recorded at room temperature on a BRUKER AC 250 or Avance III 500 operating at 400 or 500, 100 or 125, 425 or 470, and 54 MHz for ^{1}H, ^{13}C, ^{19}F, and ^{11}B respectively. Data are listed in parts per million (ppm) and are reported relative to tetramethylsilane (^{1}H and ^{13}C); residual solvent peaks of the deuterated solvents were used as internal standards. Mass spectra were realized in Spectropole de Marseille (http://www.spectropole.fr/) and at Faculty of Chemistry and Chemical Technology, University of Ljubljana on TOF LC/MS spectrometer. Solid-state spectra and fluorescence quantum yields were measured using an integrating sphere. UV-Vis-absorption spectra were measured on a Varian Cary 50. Emission spectra were measured on a Horiba-JobinYvon Fluorolog-3 spectrofluorimeter that was equipped with a three-slit double-grating excitation and a spectrograph emission monochromator with dispersions of 2.1 nm.mm^{-1} (1200 grooves.mm^{-1}). Steady-state luminescence excitation was done using unpolarized light from a 450W xenon CW lamp and detected at an angle of 90° for dilute-solution measurements (10 mm quartz cell) and with a red-sensitive Hamamatsu R928 photomultiplier tube. Special care was taken to correct emission spectra that were obtained with the latter device. The detector was corrected according to the procedure described by Parker *et al.*.[37] The observed photomultiplier output A_1 was recorded at a wavelength λ, which corresponds to the apparent emission spectrum. A_1 is given by $A_1 = (F_1)(S_1)/\lambda^2$, where F_1 and S_1 are, respectively, the corrected emission spectrum and the spectroscopic sensitivity factor of the monochromator-photomultiplier setup.

To calculate S_1, we used 4-N,N-dimethylamino-4'-nitrostilbene (DMANS) as a standard fluorophore for which its corrected emission spectrum has been precisely determined.[38] Luminescence quantum yields (Φ_f) were measured in dilute DCM solutions with an absorbance below 0.1 using $\Phi_{fx}/\Phi_{fr} = [OD_r (\lambda)/OD_x(\lambda)][I_x/I_r][n_x/n_r]$. where $OD(\lambda)$ is the absorbance at the excitation wavelength (λ), n the refractive index, and I the integrated luminescence intensity. The "r" and "x" subscripts stand for reference and sample, respectively. The luminescence quantum yields were not corrected by the refractive indices. We used as reference ruthenium trisbipyridine bischloride ($\Phi_{fr} = 0.021$ in water).[39]

Time-resolved fluorescence measurements were carried out using a Noncolinear Optical Parametric Amplifier (NOPA) pumped by a fiber femtosecond laser (Amplitude Systemes Tangerine), and a streak camera (Hamamatsu PLP system) with a time resolution of about 10 ps. The pulse duration was 100 fs and the repetition rate was 10 kHz. The pumping intensity was controlled using a set of neutral densities. The PL was collected at the magic angle between the polarization of the excitation light and the polarization of the detected polarized light in order to avoid any polarization anisotropy effect; the reported τ values are given with an estimated uncertainty of about 10%.

Cyclic voltammetric (CV) data were acquired using a BAS 100 Potentiostat (Bioanalytical Systems) and a PC computer containing BAS100W software (v2.3). A three-electrode system with a Pt working electrode (diameter 1.6 mm), a Pt counter electrode and an Ag/AgCl (with 3M NaCl filling solution) reference electrode was used. [(n-Bu)$_4$N]PF$_6$ (0.1 M in dichloromethane) served as an inert electrolyte. Cyclic voltammograms were recorded at a scan rate of 100 mV.s^{-1}. Ferrocene was used as internal standard.[40]

All DFT/TD-DFT calculations were carried with the Gaussian09 (version D.01) program,[41] tightening self-consistent field convergence thresholds (10^{-10} au) and geometry optimization (10^{-5} au) convergence thresholds. For all calculations, the hybrid PBE0[42, 43] functional has been used. The 6-311G(2d,p) atomic basis set has been employed for geometry and frequency calculations, whereas the 6-311+G(2d,p) atomic basis set was used for determining electronic transitions. Solvent effects were included according to the Polarizable Continuum Model[44] using a linear-response nonequilibrium approach for the TD-DFT step.[45, 46]

Synthetic procedures

General synthetic procedure

A pre-cooled solution (−78 °C) of phenylacetylene (326 mg, 3.2 mmol) in dry THF (10 mL) was treated dropwise with the *n*-BuLi solution (1.6M, 2.0 mL, 3.2 mmol). Reaction mixture was stirred at −78 °C for 30 minutes and then dropwise added to the pre-cooled (−78 °C) solution of 4-ethoxy-2,2-difluoro-8-methoxy-5,6-dihydro-2*H*-2λ^4,3λ^3-naphtho[1,2-*d*][1,3,2]dioxaborinine (977 mg, 3.30 mmol) in dry THF (20 mL). The reaction mixture was stirred at −78 °C for 30 minutes and then quenched with HCl (1M, 2.5 mL). The product was extracted into DCM (3 × 10 mL), dried over MgSO$_4$ and evaporated.

2,2-difluoro-8-methoxy-4-(phenylethynyl)-5,6-dihydro-2*H*-2λ^4,3λ^3-naphtho[1,2-*d*][1,3,2]dioxaborinine (**2**)

The crude product was treated with Et$_2$O (10 mL) and filtered of yielding (912 mg, 81%) of pure product. R_f = 0.22 (petroleum ether–EtOAc = 5/3). IR (KBr, cm^{-1}): 2200, 1600, 1543, 1500, 1484, 1461, 1432, 1391, 1321, 1281, 1249, 1138, 1076, 1041, 1015. ^{1}H NMR (500 MHz): δ 8.14 (d, ^3J = 9.0 Hz, 1H), 7.64–7.62 (m, 2H), 7.53–7.49 (m, 1H), 7.44–7.41 (m, 2H), 6.91 (dd, ^3J = 9.0, ^4J = 2.5 Hz, 1H), 6.80 (d, ^4J = 2.5 Hz, 1H), 3.01–2.92 (m, 4H). ^{11}B NMR (53.7 MHz): δ 0.75. ^{19}F NMR (470.4 MHz): δ −140.2. ^{13}C NMR (75.5 MHz): δ 179.2, 166.4, 161.9, 147.6, 133.0, 131.5, 131.4, 128.8, 120.9, 119.7, 114.0, 113.6, 110.7, 104.1, 84.1, 55.9, 28.1, 22.7. HRMS (ESI+, [MNH$_4$]$^+$) Calcd for C$_{20}$H$_{19}$BF$_2$NO$_3$: 370.1426. Found 370.1422.

4-((4-chlorophenyl)ethynyl)-2,2-difluoro-8-methoxy-5,6-dihydro-2*H*-2λ^4,3λ^3-naphtho[1,2-*d*][1,3,2]dioxaborinine (**3**)

The crude product was recrystallized from MeCN yielding (853 mg, 69%) pure product. R_f = 0.27 (petroleum ether–EtOAc = 5/3). IR (KBr, cm^{-1}): 2194, 1621, 1570, 1536, 1399, 1154, 1062, 823. ^{1}H NMR (500 MHz): δ 8.16 (d, ^3J = 9.5 Hz, 1H), 7.56 (AA'BB', ^3J = 8.5 Hz, 2H), 7.42 (AA'BB', ^3J = 8.5 Hz, 2H), 6.92 (dd, ^3J = 9.0, ^4J = 2.5 Hz, 1H), 6.79 (d, ^4J = 2.5 Hz, 1H), 3.93 (s, 3H), 3.01–2.91 (m, 4H). ^{11}B NMR (53.7 MHz): δ −0.67. ^{19}F NMR (470.4 MHz): δ −159.26. ^{13}C NMR (75.5 MHz): δ 179.5, 166.5, 161.4, 147.7, 137.8, 134.1, 131.7, 129.3, 121.0, 118.2, 114.0, 113.6, 110.8, 102.4, 84.8, 55.9, 28.1, 22.7. HRMS (ESI+, [M-F]$^+$) Calcd for C$_{20}$H$_{13}$BClFO$_3$: 367.0709. Found 367.0697. Anal. Calcd for: C$_{20}$H$_{14}$BClF$_2$O$_3$: C, 62.14; H, 3.65. Found: C, 62.38, H, 3.55.

2,2-difluoro-4-(*p*-tolylethynyl)-5,6-dihydro-2*H*-2λ^4,3λ^3-naphtho[1,2-*d*][1,3,2]dioxaborinine (**4**).

The crude product was treated with DCM (3 mL) and filtered off yielding (822 mg, 73%) pure product. R_f = 0.20 (petroleum ether–EtOAc = 5/3). IR (KBr, cm^{-1}): 2188, 1687, 1583, 1543, 1511, 1360, 1345, 1331, 1297, 1276, 1260, 1245, 1225, 1165, 1144, 1018. ^{1}H NMR (500 MHz): δ 8.16 (d, ^3J = 7.5 Hz, 1H), 7.61–7.57 (m, 3H), 7.41 (dd, ^3J = 7.5, ^3J =7.5 Hz, 1H), 7.32 (d, ^3J = 7.5 Hz, 1H), 6.95 (AA'BB', ^3J = 9.0 Hz, 2H), 3.04–2.94 (m, 4H). ^{11}B NMR (53.7 MHz): δ 0.84. ^{19}F NMR (470.4 MHz): δ −139.6. ^{13}C NMR (75.5 MHz): δ 179.0, 165.1, 162.7, 143.9, 135.7, 135.5, 128.4, 128.4, 128.3, 127.7, 114.7, 111.2, 110.9, 107.7, 84.6, 55.6, 27.6, 22.5. HRMS (ESI+, [MNH$_4$]$^+$) Calcd for C$_{20}$H$_{19}$BF$_2$NO$_3$: 370.1426. Found 370.1426.

4-((2,2-difluoro-5,6-dihydro-2*H*-2λ^4,3λ^3-naphtho[1,2-*d*][1,3,2]dioxaborinin-4-yl)ethynyl)-*N*,*N*-dimethylaniline (**5**)

The crude product was treated with EtOAc (10 mL) and filtered off under reduced pressure yielding (596 mg, 51%) pure product. R_f = 0.10 (petroleum ether–EtOAc = 5/3). IR (KBr, cm$^-$^{1}): 2162, 1599, 1530, 1483, 1453, 1346, 1330, 1275, 1175, 1135, 1060, 1027. ^{1}H NMR (500 MHz): δ 8.145 (d, ^3J = 7.5 Hz, 1H), 7.57–7.51 (m, 3H), 7.40 (dd, ^3J = 7.5, ^3J =7.5 Hz, 1H), 7.29 (d, ^3J = 7.5 Hz, 1H), 6.67 (AA'BB', ^3J = 9.0 Hz. 2H) 3.09 (s, 6H), 3.02–2.90 (m, 4H). ^{11}B NMR (53.7 MHz): δ 0.84. ^{19}F NMR (470.4 MHz): δ –140.2. ^{13}C NMR (75.5 MHz): δ 176.9, 165.6, 152.5, 143.3, 135.7, 134.9, 128.8, 128.2, 128.0, 127.5, 112.7, 111.7, 110.0, 104.8, 86.79, 40.1, 27.7, 22.4. HRMS (ESI+, [MH]$^+$) Calcd for C$_{21}$H$_{19}$BF$_2$NO$_2$: 366.1477. Found 366.1478.

2,2-difluoro-4-((6-methoxynaphthalen-2-yl)ethynyl)-5,6-dihydro-2H-2λ^4,3λ^3-naphtho[1,2-d][1,3,2]dioxaborinine (**6**)

The crude product was recrystallized from DCM yielding (850 mg, 66%) pure product. R_f = 0.15 (petroleum ether–EtOAc = 5/3). IR (KBr, cm^{-1}): 2185, 1619, 1601, 1547, 1504, 1477, 1453, 1434, 1348, 1328, 1245, 1041, 1023, 855. ^{1}H NMR (500 MHz): δ 8.19 (d, ^3J = 8.0 Hz, 1H), 8.16 (s, 1H), 7.78 (d, ^3J = 8.0 Hz, 1H), 7.77 (d, ^3J = 8.0 Hz, 1H), 7.62–7.58 (m, 2H) 7.43 (dd, ^3J = 8.0, ^3J =8.0 Hz, 1H), 7.33 (d, ^3J = 7.5 Hz, 1H), 7.23 (dd, ^3J = 9.0, ^4J =2.0 Hz, 1H), 7.15 (d, ^4J = 2.0 Hz, 1H), 3.96 (s, 3H), 3.08–2.99 (m, 4H). ^{11}B NMR (53.7 MHz): δ 0.86. ^{19}F NMR (470.4 MHz): δ –139.5. ^{13}C NMR (75.5 MHz): δ 179.3, 164.9, 159.9, 144.0, 136.2, 135.8, 134.9, 130.1, 128.9, 128.44, 128.40, 128.4, 128.1, 127.8, 127.5, 120.3, 114.0, 111.2, 107.6, 106.0, 84.7, 55.5, 27.6, 22.5. HRMS (ESI+, [MNH$_4$]$^+$) Calcd for C$_{24}$H$_{21}$BF$_2$NO$_3$: 420.1583. Found 420.1584.

2,2-difluoro-8-methoxy-4-(phenanthren-9-ylethynyl)-5,6-dihydro-2H-2λ^4,3λ^3-naphtho[1,2-d][1,3,2]dioxaborinine (**7**)

The crude product was recrystallized from DCM yielding (1.012 mg, 70%) pure product. R_f = 0.20 (petroleum ether–EtOAc = 5/3). IR (KBr, cm^{-1}): 2906, 2839, 2338, 1611, 1573, 1531, 1477, 1426, 1283, 1026. ^{1}H NMR (500 MHz): δ 8.74–8.69 (m, 2H), 8.42–8.40 (m, 1H), 8.27 (s, 1H), 8.20 (d, ^3J = 9.0 Hz, 1H), 7.94 (d, ^3J = 8.0 Hz, 1H), 7.79–7.74 (m, 3H), 7.67 (t, ^3J = 7.5 Hz, 1H), 6.94 (dd, ^3J = 9.0 Hz, ^4J = 2.5, 1H), 6.82 (d, ^4J = 2.5 Hz, 1H), 3.94 (s, 3H), 3.13–3.06 (m, 4H). ^{11}B NMR (53.7 MHz): δ 0.85. ^{19}F NMR (470.4 MHz): δ –140.2. ^{13}C NMR (75.5 MHz): δ 179.4, 166.4, 162.0, 147.5, 136.2, 131.6, 130.6, 130.3, 130.2, 130.0, 129.4, 129.3, 127.8, 127.4, 126.5, 123.1, 122.9, 121.1, 116.4 113.9, 113.7, 110.7, 102.9, 88.5, 55.9, 22.9, 28.2. HRMS (ESI+, [M-F]$^+$) Calcd for C$_{28}$H$_{19}$BFO$_3$: 432.1442. Found 432.1445.

2,2-difluoro-4-(4-methoxystyryl)-5,6-dihydro-2*H*-2λ⁴,3λ³-naphtho[1,2-*d*][1,3,2]dioxaborinin-3-ium-2-uide (**MC4**)

The crude product was solubilized in a minimum of DCM (10 mL), precipitated with Et₂O and filtered off yielding (0.715 mg, 62%) pure product. R_f = 0.2 (petroleum ether–DCM = 2/1). ¹H NMR (400 MHz): δ 8.19-8.16 (m, 2H), 7.64 (d, ^3J = 8.8 Hz, 2H), 7.55 (dt, ^3J = 7.3 Hz, ^4J = 1.2 Hz, 1H), 7.40 (t, ^3J = 7.9 Hz, 1H), 7.29 (d, ^3J = 8.0 Hz, 1H), 6.96 (m, 3H), 3.89 (s, 3H), 3.02-2.88 (m, 4H). ¹³C NMR (100 MHz): δ 185.7, 176.4, 161.1, 141.7, 140.2, 132.7, 132.3, 129.7, 128.2, 127.6, 126.9, 126.4, 116.7, 114.3, 106.6, 55.3, 28.3, 22.5. HRMS (ESI+, [M+Na]⁺) Calcd for $C_{20}H_{17}BF_2O_3Na^+$: 377.1137. Found 377.1139.

2,2-difluoro-4-(2-(6-methoxynaphthalen-2-yl)vinyl)-5,6-dihydro-2*H*-2λ⁴,3λ³-naphtho[1,2-*d*][1,3,2]dioxaborinin-3-ium-2-uide (**MC6**)

The crude product was solubilized in a minimum of DCM (10 mL), precipitated with Et₂O and filtered off yielding (0.862 mg, 78%) pure product. R_f = 0.4 (petroleum ether–DCM = 1/1). ¹H NMR (400 MHz): δ 8.30 (d, ^3J = 15.2 Hz, 1H), 8.16 (d, ^3J = 7.6 Hz, 1H), 8.00 (s, 1H), 7.80 (d, ^3J = 8.8 Hz, 1H), 7.77-7.71 (m, 2H), 7.55 (dt, ^3J = 7.6 Hz, ^4J = 1.6 Hz, 1H), 7.39 (d, ^3J = 7.6 Hz, 1H), 7.29 (d, ^3J = 7.6 Hz, 1H), 7.20 (dd, ^3J = 8.8 Hz, ^4J = 2.4 Hz, 1H), 7.11-7.15 (m, 2H), 3.95 (s, 3H), 3.01-2.91 (m, 4H). ¹³C NMR (100 MHz): δ 177.5, 159.8, 148.9, 143.0, 136.8, 135.7, 134.9, 132.4, 130.8, 129.8, 129.2, 128.7, 128.0, 127.9, 127.6, 124.5, 119.9, 115.7, 106.2, 55.6, 27.6, 21.3. HRMS (ESI+, [M+Na]⁺) Calcd for $C_{24}H_{19}BF_2O_3Na^+$: 427.1293. Found 427.1294.

3. Results and discussion

Synthesis and X-Ray crystal structures

The synthesis of the model hemicurcuminoid boron difluorides was achieved as reported elsewhere[34] using benzoylacetone or 2-acetyl-1-tetralone as starting materials, boron oxide as chelate for the acetylacetone moiety and the appropriate aldehyde in an aldol-like extension of the conjugation. The compounds containing acetylene function were prepared in a similar way that was reported previously.[36]

Crystals suitable for X-Ray diffraction of **3**, **4**, **6** and **7** were obtained by crystallization from DCM or mixture of solvents DCM and EtOAc. Detailed crystallographic parameters are listed in Table S1 in the supporting information (SI). While **3** (P-1) crystallizes in the triclinic system, **4**, **6** and **7** (P21/c) crystallize in a monoclinic space group. In addition, the

dioxaborine rings in these four compounds present almost the same bond lengths (Table S2) independently of the substituent pattern of the tetralone phenyl ring and the phenyl acetylenic ring. We defined ψ as the angle between the plane of phenyl ring belonging the tetralone and that of the terminal aryl group. While complexes **3** and **7** show ψ values of 2.0° and 3.8°, respectively, and are therefore planar, complexes **4** and **6** are distorted with ψ values of 20.1° and 37.2°, respectively. It has to be noted that the endocyclic C-C bond of the Acac moiety is always slightly longer than the exocyclic C-C bond (1.39-1.40 Å *versus* 1.37-1.38 Å, Table S2), suggesting that the latter has a stronger double bond character. This localization of the double bond is also consistent with the C-O distances that are 1.29-1.30 Å for the endocyclic C-O *versus* 1.31 Å (for the exocyclic C-O (Table S2).

All borondifluoride complexes are π-stacked forming head-to-tail dimers with the dioxaborine unit of one molecule lying above the triple bond of the donor group (side B) of the adjacent molecule. The intra-dimer distances between average molecular planes are short for the four compounds, close to the van der Waals contact distance, indicating a tight packing as generally observed for dipolar dyes in the crystal. For **3**, this distance equals 3.547 Å, two adjacent dimers being separated by 3.592 Å. For dyes **7** and **4**, the intra-dimer distance are shorter (3.382 and 3.509 Å, respectively). Dye **6** shows the most densely packed solid with an interplanar distance of 3.173 Å.

Electrochemistry

The electrochemical potentials of the first oxidation and reduction processes of the complexes were determined in dichloromethane (DCM) containing 0.1 M of (n-Bu)$_4$NPF$_6$. The data are collected in Table 1 ($E_{1/2}$ *vs.* ferrocene/ferrocenium). The first oxidation can be attributed to the electron donor moiety of the systems (side B) while the first reduction corresponds to the acceptor moiety (dioxaborine ring).

As can be seen from Table 1, by comparing **4** and **6** with **MC4** and **MC6**, one notices that the introduction of a triple bond results in a less negative reduction potential (by 40 and 70 mV, respectively). This is associated with a higher oxidation potential for **4** and **6**. These effects can be attributed to the acceptor character of the triple bond. The same trend is observed for the reduction of **M1** *versus* **M'1** (one can notice that, due to the absence of donor group on those latter dyes, no oxidation could be detected). The bridging of the dioxaborine ring *via* the CH$_2$-CH$_2$ unit makes the tetralone-based **MC4** and **MC6** easier to reduce compared to **M'4** and **M'6**, but the reverse effect is noticed for the ethynylene compounds **1** and **M1**. In the

same time, an easier oxidation was observed for **MC4** and **MC6**, yielding a much lower electrochemical gap for the dyes containing tetralone. Finally, as noticed in the BF$_2$-hemicurcuminoid series,[34] increasing the strength of the electron donor moiety results in lower oxidation potential values. This effect is accompanied by a slight cathodic shift of the reduction potential.

It can also be seen from Table 1 that the Gibbs free energy calculated for photoinduced electron transfer using the Rehm-Weller equation is negative for most of the borondifluoride complexes, which indicates a thermodynamically-allowed photoinduced electron transfer process which would occur from the donor moiety (side B) to the dioxaborine part in these molecules in polar medium such as DCM solution.

Table 1. Oxidation and reduction half-wave potential values for the studied dioxaborine derivatives (10µM) in dichloromethane solution using tetrabutylammonium hexafluorophosphate as electrolyte (100µM), the values are given in volt *vs.* Fc/Fc$^{+\bullet}$.

Cmpd	$E^{red}(1)$ / V	$E^{ox}(1)$ / V	$E_g,$ ^{a} / V	E_{0-0} ^{b} / eV	ΔG^c / eV
1	-1.21	-^{d}	-^{d}	2.76	-^{d}
2	-1.33	1.51	2.84	2.67	0.1
3	-1.27	1.46	2.73	2.63	0
4	-1.27	1.47	2.74	2.62	0
5	-1.35	0.65	2.00	2.16	-0.2
6	-1.18	1.22	2.40	2.51	-0.2
7	-1.26	1.04	2.30	2.53	-0.3
M1	-1.17	-^{d}	-^{d}	2.97	-^{d}
MC4	-1.31	1.17	2.48	2.45	-0.1
MC6	-1.25	1.02	2.27	2.37	-0.2
M'1	-1.22	-^{d}	-^{d}	2.83	-^{d}
M'4	-1.40	1.33	2.73	2.58	0.1
M'6	-1.32	1.07	2.39	2.49	-0.2

^{a} E_g, Electrochemical HOMO-LUMO gap $\Delta E_g = (E_{1/2}^{ox})_1 - E_{1/2}^{red}$, ^{b} Optical gap determined from the UV-visible absorption spectra. ^{c} $\Delta G = E(D+/D) - E(A/A-) - E_{00} - e^2/\varepsilon d$. ^{d} no oxidation was observed in DCM. ^{d} not possible to determine.

Photophysical properties in solution & (TD-)DFT calculations

The optical properties of the dyes were measured in DCM and the spectroscopic data are collected in Table 2. The UV-vis electronic spectra displayed large molar absorption coefficient values (ε) around 40000M^{-1}cm^{-1}. They all exhibit a red shift of the lowest energy transition band when solvent polarity increases. This positive solvatochromic effect is attributed to the charge transfer character or the electronic transition from the ground- to the

Franck-Condon excited state,[47] as observed for boron difluoride complexes of chalcones,[48, 49] curcuminoids[30, 35, 50] and hemicurcuminoids.[34] This behaviour is confirmed by the results of (TD-)DFT calculations (see computational details). Dyes **2** and **3** show a small shift like compounds **1**, **M1** and **M'1** lacking the donor group at the B side. In those cases, the HOMO and LUMO electronic densities, not showing the typical donor-acceptor behaviour (*vide infra*), confirm the absence of any push-pull character (see Figure 1) which can be rationalized by the smaller conjugation pathway when compared to **4**. **7** is slightly different since the HOMO and LUMO show a delocalisation from the phenanthrene moiety to the carbonyl group evidencing a partial CT character.

Given the odd number of p_z carbon atomic orbitals involved in the conjugation, we can consider that these chromophores as cyanine-like systems. Figure 1 shows the HOMO-1, HOMO, LUMO and LUMO+1 representations for **1**, **M1**, **M'1** and **7**. First, we clearly notice the expected π-π^* nature of the excited states, and that both vinyl and ethynyl linkers, allow an effective conjugation between the donor and acceptor moieties. As a consequence, the HOMO orbital is mainly located on the lateral arms while the LUMO is spread over the central borondifluoride core.
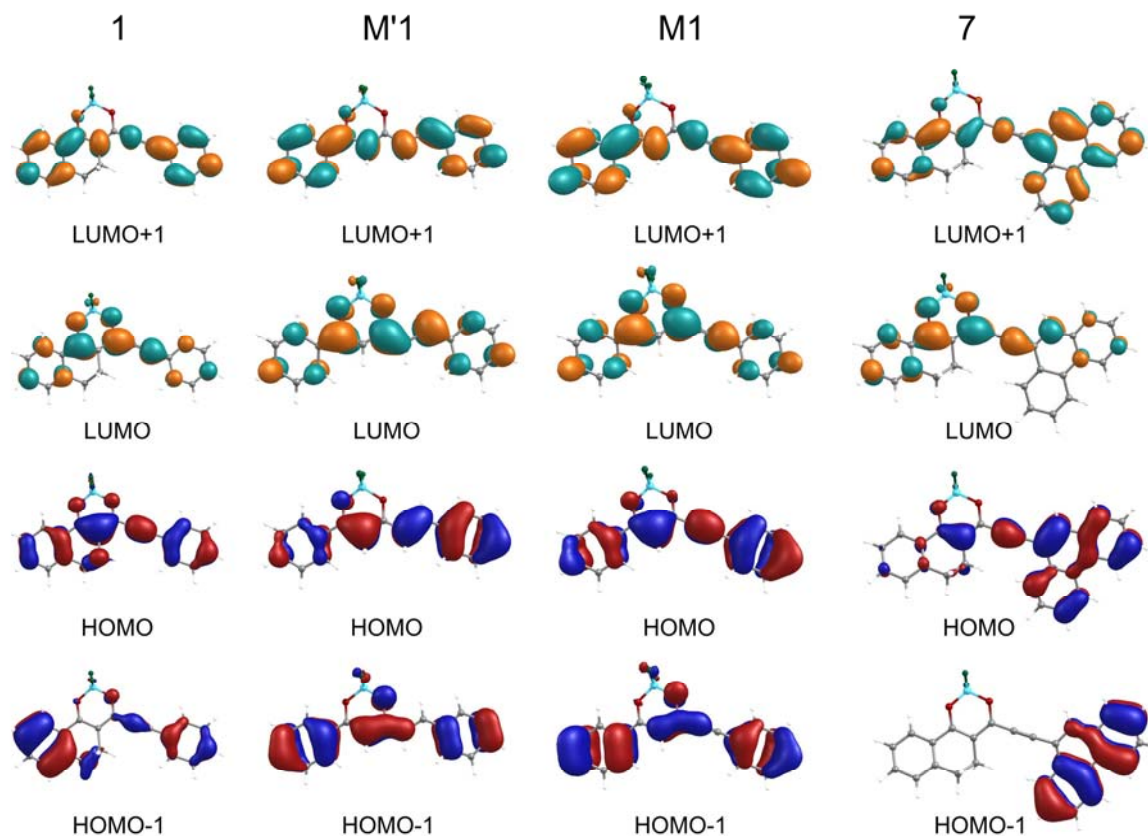
Figure 1. HOMO, HOMO-1, LUMO and LUMO+1 of chromophores **1**, **M'1**, **M1** and **7** (threshold 0.03 a.u.).

The calculated absorption data (Table S3) reveal a dominating HOMO-LUMO character of the S_0-S_1 excitations that are associated with large oscillator strengths ranging from 1.051 (**1**) to 1.492 (**MC6**). Additionally, the band gap energies are presented in Table S4 and Figure S11, where it can be noticed the higher values obtained for **1** (3.7 eV), **M'1** (3.8 eV) and **M1** (3.9 eV) that can be attributed to the least donating behaviour of the phenyl ring in comparison to other substituents, resulting in lower HOMO energies. Conversely, the strong electron donor character of the dimehtylaminophenyl group attached to the BF_2 moiety through an ethynyl linker makes **5** the chromophore with the smallest band gap (3.0 eV). Remarkably, the calculated bandgap trend is in good agreement with those obtained by electrochemical and optical methodologies (Table 1).

The absorption maximum is red-shifted when increasing the donor strength of the B part up to 514 nm for the dimethylamino donor **5**. When comparing to the dyes containing a double bond instead of the triple bond (**MC4** and **MC6** compared to **4** and **6**, respectively), it appears that **MC4** and **MC6** are red shifted by 21-22 nm as a result of the better conjugation pathway. This is also in line with the better acceptor character of the triple bond and the electrochemical trend observed (*vide supra*). In addition, comparing **MC4** and **MC6** to hemicurcuminoid boron difluoride **M'4** and **M'6**,[34] a red-shift of the absorption of the tetralone containing boron difluoride dyes **MC4** and **MC6** is observed which is in line with the more planar structure induced by the cyclic structure of the tetralone.

Table 2. Spectroscopic data and photophysical properties of the compounds recorded in DCM at room temperature[a] and fluorescence properties of the powder.

| compound | UV-vis | | Fluorescence | | | | | | | | | |
| | DCM | | DCM | | | | | | | Powder | |
	λ_{abs}	ε_{max}	λ_{em}	$\Delta \nu_{ST}$	Φ_f	$\Phi_f \times \varepsilon$	τ_f	k_f	k_{nr}	λ_{em}	Φ_f
1	431	40270	452	1078	0.83	33424	2.79	3.0	0.6	589	0.10
2	443	41280	469	1251	0.80	33024	2.61	3.1	0.8	567	0.23
3	445	39600	472	1285	0.72	28512	2.53	2.8	1.1	591	0.18
4	446	42150	493	2138	0.145	6112	1.49	1.0	5.7	611	0.16
5	514	47520	-	-	-	-	-	-	-	742	0.02
6	457	40900	566	4214	0.16	6544	1.69	1.0	5.0	630	0.07
7	465	39990	500	1505	0.425	16996	1.33	3.2	4.3	650	0.07
M1	401	38730	420	1128	0.43	16654	0.94	4.6	6.1	606	0.20
MC4	467	39580	515	1996	0.04	1583	0.24	1.6	38.4	635	0.13

MC6	479	40150	564	3146	0.33	13250	1.60	2.1	4.2	666	0.06
M'1	398	53950	443	2552	0.02	1079	0.10	2.0	98.0	544	0.24
M'4	444	42410	506	2760	0.055	2332.5	-	-	-	636	0.11
M'6	456	50410	566	4262	0.43	21676	2.53	1.7	2.3	575	0.08

[a] Absorption maximum wavelengths λ_{abs} (nm), molar absorption coefficients ε_{max} (M^{-1} cm^{-1}), fluorescence maximum wavelengths λ_{em} (nm), Stokes shifts $\Delta \nu_{ST}$ (cm^{-1}), fluorescence quantum yields Φ_f, brightness Φ_f x ε (M^{-1} cm^{-1}), fluorescence lifetimes τ_f (ns), radiative k_f (10^8 s^{-1}) and non-radiative k_{nr} = (1 - Φ_f)/τ_f (10^8 s^{-1}) rate constants

All compounds but **5** were found to be emissive in DCM solution with fluorescence quantum yields spanning from 2% to 83% (Table 2). Fluorescence emission was found to decay monoexponentially. Remarkably, when increasing the donor strength on the B side, the fluorescence quantum yield decreases until no emission could be detected for **5** in DCM. To get more insight into the excited state properties, fluorescence emission spectroscopy was also performed using solvent of various polarities (Figure S12 to Figure S22). The Lippert-Mataga plots are depicted in Figures S23-S25. For **5**, fluorescence was efficient in solvents of low polarity only. We therefore used those data to get the Lippert-Mataga slope.

The dyes lacking a donor group (*i.e.* **1**, **M1** and **M'1**) or methoxy donors on the tetralone A side (*i.e.* **2** and **3**), show low value of the slopes proving that the dipole moment of the excited state is similar to that of the ground state which is line with π-π* character of the S_0-S_1 transition. **7** shows a large slope value which can be attributed to the donor character of the phenanthrene moiety. For all other dyes, the Lippert-Mataga slopes are large revealing that the excited-state dipole moment is much larger than their ground-state counterparts for such push-pull systems.[51-53] For instance, **5** presents the largest slope of those dyes (*ca.* 23600) indicating a variation of dipole moment of the order of *ca.* 10D.

Compounds **1** and **M1** containing the triple bond are more emissive than **M'1** in all solvents. The photophysical data (Tables 2, S5 and S9) show a large value of the non-radiative deactivation constant for the latter. The singlet excited state of both **M1** and **M'1** exhibit a very short lifetime (subnanosecond) as compared to the bridged dye **1**. These observations and the fact that absorption and emission spectra are redshifted may indicate a more planar geometry for the bridged compound **1**. Further, we found that **M1** is more emissive than **M'1** which might be attributed to her planarity of the triple bond containing dye in its excited state which results in a smaller value of k_{nr}. Except for a bathochromic shift of both absorption and emission, the photophysical properties (fluorescence quantum yield and lifetime) of **2** and **3** in solution are found to be very similar to those of **1**. Indeed **1** - **3** are highly emissive in all

investigated solvents with fluorescence quantum yields ranging between 60 % and nearly unity.

The fluorescence emission spectra of **1**, **4**, **5** and **6** in solution show a bathochromic shift when the electron donor strength of the *para*-substituent increases. This is due to the push-pull nature of the dyes giving a Lippert-Mataga slope increasing with the donor strength increases (Figure S24b). Consistently, dramatic solvatochromic changes are noticed for **4** and **5** as compared to **1** and the fluorescence quantum yields decrease considerably for **4** and **5** when solvent polarity increases. Here, it can also be noted that the fluorescence spectrum of **4** starts to show a broad and structureless emission at low energy in solvents such as acetone and acetonitrile (Figure S15b) while, for **5**, starting from chloroform (Figure S16b) and in 1,1,1-trichloroethane (Figures 2f and S16b), a broad and weak emission is observed. Those emissions might correspond to the radiative recombination process from a slightly emissive photo-induced electron transfer state (Figure S10). This effect already has been observed for a similar compound featuring double bond instead of the triple bond.[34]
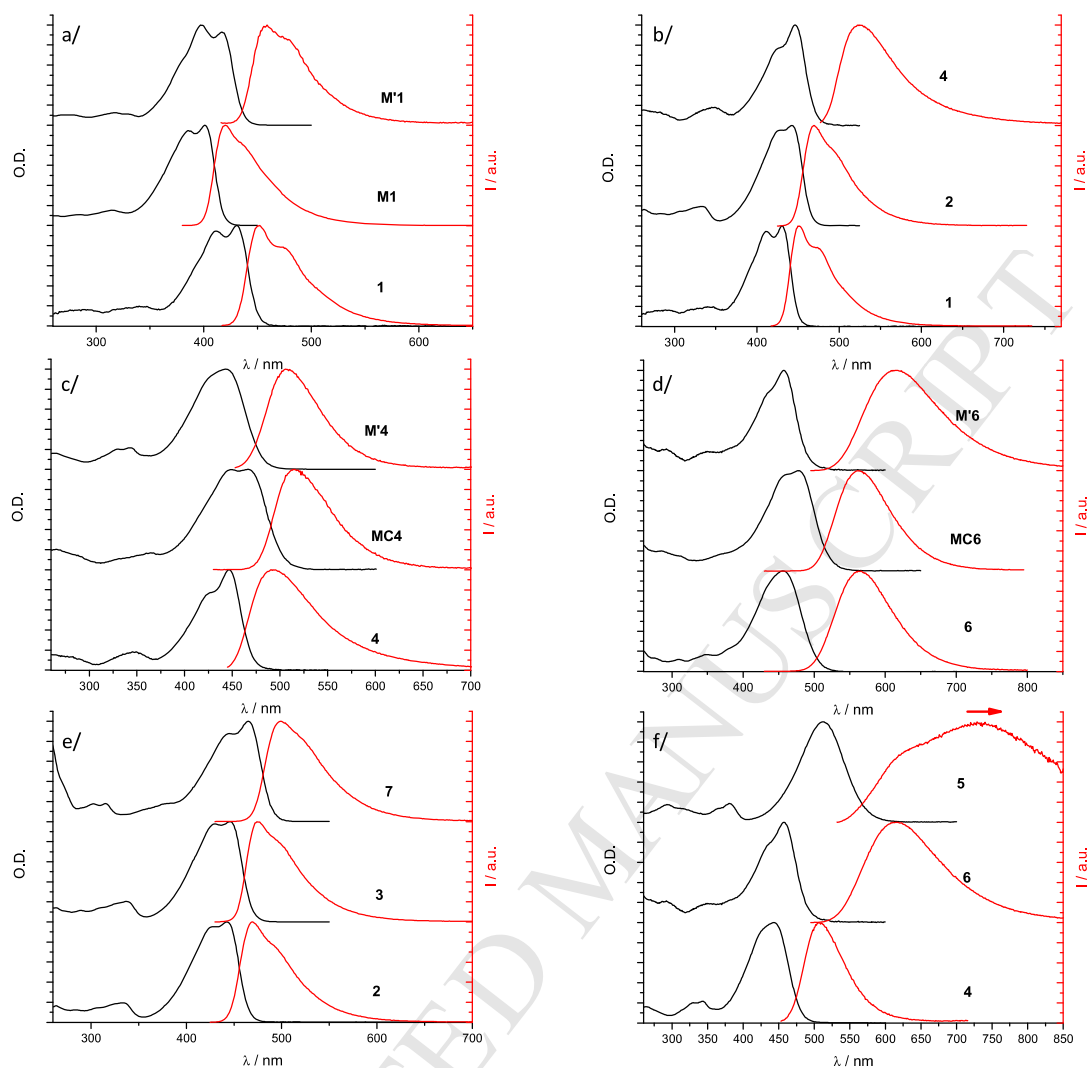
Figure 2. UV/visible absorption spectra (▬) and fluorescence spectra (▬) in DCM of a/ **1**, **M1** and **M'1**, b/ **1**, **2** and **4**, c/ **4**, **MC4** and **M'4**, d/ **6**, **MC6** and **M'6**, e/ **2**, **3** and **7**, and f/ **4**, **6** and **5**. Note that no emission was recorded in DCM solution, the emission of **5** presented on the figure correspond to the emission in 1,1,1-trichloroethane, the arrow means that the emission in DCM would be even more red shifted.

It is interesting to note that dye **4** containing the ethynylene unit exhibits spectra that are blue shifted as compared to the vinylene analogue **MC4**. The same trend is observed for **6** and **MC6** but in solvents of low to moderate polarity only. This effect has already been observed in other push-pull molecules[54] and π-conjugated systems containing C(sp)/C(sp^2) bonds.[55] The larger value of the Stokes shift in **4** and **6** relative to **MC4** and **MC6** is also consistent with previous works.[54-56] The values of the fluorescence quantum yield and lifetime for **4** and **6** (Tables S6 and S7) show a similar trend characterized by a decrease of both Φ_f and τ_f leading to a decrease of k_f and an increase of k_{nr} for **4** (more or less constant for

6) when the solvent polarity increases. This may be attributed to a more pronounced charge transfer character of the emitting state for the ethynylene-containing molecules. The trend is opposite for the bridged vinylene analogues, **MC4** and **MC6** (Table S10), for which k_f slightly increases and k_{nr} decreases when the solvent polarity increases. These effects may arise from a more allowed radiative transition in polar solvents associated with a planarization of the excited-state geometry. This is particularly the case for the naphthalenic compound **MC6** for which the fluorescence quantum yield is one order of magnitude larger in acetonitrile (almost 50 %) than in cyclohexane (5 %).[34] The value of k_{nr} for **MC4** is 5 to 10 fold larger than that for **MC6** depending on the solvent. The redshift of absorption and emission spectra of dyes **MC4** and **MC6** as compared to **M'4** and **M'6**, respectively, in DCM and other solvents, can originate from the occurrence of a more planar structure imposed by the tetralone unit.[34]

Solid state photophysical properties

We also investigated the emission properties of the boron difluoride complexes in the solid state (powder form) by measuring their emission spectra and their fluorescence quantum yields. All compounds were found to be emissive in the solid state (Table 2, Figure 2) with fluorescence quantum yields ranging from 2% to 24%. The dyes emit mainly in the visible with the exception of **5** that reaches the NIR region of the spectrum.

The shape of spectra of the boron difluoride **2**, **3**, **7** and **M1** (Figures 3a and 3b) is unsymmetrical revealing the occurrence of different chromophore populations in the powder samples while all other spectra displayed a structureless emission band that suggests that emission originated from a single population of complexes in the thin films (Figure 3).

It is interesting to note that boron difluoride complexes **4**, **MC4** and **5** display fluorescence with quantum yields higher than in DCM solution, which demonstrates that those dyes show aggregation enhanced emission (AIE). For **4** and **MC4**, the emission is red shifted by more than 100 nm with respect to the spectra recorded in DCM. The case of **5** is spectacular since no detectable emission was observed in DCM solution and aggregation-induced NIR emission (742 nm) is clearly observed albeit the fluorescence quantum yield remains low (2%). For all other dyes, despite the occurrence of restricted intramolecular rotation in the solid, the fluorescence quantum yields are lower than in DCM solution, which indicated that aggregation-induced emission was not operative in these cases.
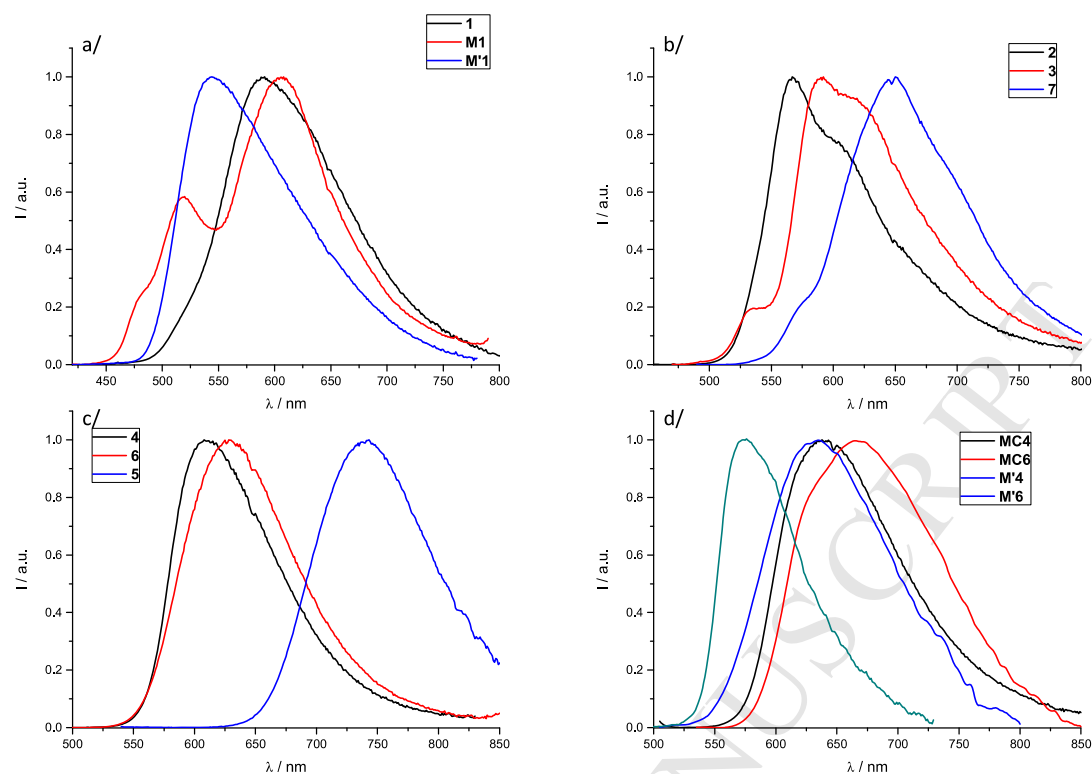
Figure 3. Normalized fluorescence spectra of powder of a/ **1** (━), **M1** (━) and **M'1** (━); b/ **2** (━), **3** (━) and **7** (━); c/ **4** (━), **6** (━) and **5** (━) and d/ **MC4** (━), **MC6** (━), **M'4** (━) and **M'1** (━).

Here, it has to be highlighted that the boron difluoride complexes **3** and **4**, which present some of the highest fluorescence quantum yield values within the series reported here (23% and 16%, respectively), are not the ones that exhibit the more tightly packed dimers compared to compounds **6** and **7**. It can be seen that **3** and **4** emit in the visible region of the spectrum at shorter wavelength (< 610nm). In contrast, the very tight packing of **6** and **7** in the crystal results in fluorescence emission at much longer wavelength (> 630 nm) but with a weaker efficiency (fluorescence quantum yield *ca.* 7%). These observations are in close agreement with the conclusions drawn by some of us on the fluorescence emission properties of a series of dipolar dyes, the boron difluoride complexes of chalcone, in the solid state.[48]

4. Conclusion

In this study, we report on the synthesis and characterization of the photophysical properties of novel boron difluoride complexes of hemicurcuminoid-related compounds containing a

triple bond. Those dyes are emissive in solution and in the solid state. Within those new dyes, the compounds that emit through an efficient CT state show low fluorescence quantum yields and solvatochromic behavior. It can be observed that, increasing the donor strength, the fluorescence quantum yield highly decreases which is attributed to the formation of a photo-induced electron transfer state. In contrast, high fluorescence quantum yields reaching 70-80% can be obtained for the dyes lacking donor groups on the B side. Similarly to hemicurcuminoid previously reported,[34] those dyes are emissive in the solid state mostly, fluorescence emission being located in the visible and reaching quantum yields of 23% for **2**. However, on the opposite of the previously reported hemicurcuminoid boron difluoride,[34] some of those dyes show aggregation induced emission effect. Those hemicurcuminoid-like dyes outperform boron difluoride of hydroxychalcone dyes in solution with much larger fluorescence quantum yields and brightness.[48] However, in the solid state, the performances of the latter (especially, their NIR emission) cannot be reached. These results provide important insights into the photophysics of the broad family of dipolar dyes based on the BF_2 complexes of bidentate O^O ligands containing a negatively-charged oxygen atom. This study is believed to serve as a strong basis for future works devoted to the development of high performance BF_2-containing dyes for applications.

5. Acknowledgements

6. References

[1] De Meulenaere E, Chen W-Q, Van Cleuvenbergen S, Zheng M-L, Psilodimitrakopoulos S, Paesen R, et al. Molecular engineering of chromophores for combined second-harmonic and two-photon fluorescence in cellular imaging. Chem Sci. 2012;3(4):984-95.

[2] Kim HM, Cho BR. Small-Molecule Two-Photon Probes for Bioimaging Applications. Chem Rev. 2015;115(11):5014-55.

[3] Wang Xiaochi CG, Cao Ruijun, Meng Lingjie. Structure and Properties of Near-Infrared Fluorescent Dyes and the Bioimaging Application. Prog Chem. 2015;27(7):794-805.

[4] Uoyama H, Goushi K, Shizu K, Nomura H, Adachi C. Highly efficient organic light-emitting diodes from delayed fluorescence. Nature. 2012;492(7428):234-8.

[5] Lin Z, Li C, Meng D, Li Y, Wang Z. Hybrid Corannulene–Perylene Dyes: Facile Synthesis and Optoelectronic Properties. Chem Asian J. 2016;11(19):2695-9.

[6] Méhes G, Pan C, Bencheikh F, Zhao L, Sugiyasu K, Takeuchi M, et al. Enhanced Electroluminescence from a Thiophene-Based Insulated Molecular Wire. ACS Macro Lett. 2016;5(7):781-5.

[7] Jiang W, Li Y, Wang Z. Tailor-Made Rylene Arrays for High Performance n-Channel Semiconductors. Acc Chem Res. 2014;47(10):3135-47.

[8] Huckaba AJ, Yella A, McNamara LE, Steen AE, Murphy JS, Carpenter CA, et al. Molecular Design Principles for Near-Infrared Absorbing and Emitting Indolizine Dyes. Chem Eur J. 2016;22(43):15536-42.

[9] Ulrich G, Ziessel R, Harriman A. The Chemistry of Fluorescent BODIPY Dyes: Versatility Unsurpassed. Angew Chem Int Ed. 2008;47(7):1184-201.

[10] Boens N, Verbelen B, Dehaen W. Postfunctionalization of the BODIPY Core: Synthesis and Spectroscopy. Eur J Org Chem. 2015;2015(30):6577-95.

[11] Kowada T, Maeda H, Kikuchi K. BODIPY-based probes for the fluorescence imaging of biomolecules in living cells. Chem Soc Rev. 2015;44(14):4953-72.

[12] Lu H, Mack J, Nyokong T, Kobayashi N, Shen Z. Optically active BODIPYs. Coord Chem Rev. 2016;318:1-15.

[13] Ge Y, O'Shea DF. Azadipyrromethenes: from traditional dye chemistry to leading edge applications. Chem Soc Rev. 2016;45(14):3846-64.

[14] Collado D, Vida Y, Najera F, Perez-Inestrosa E. PEGylated aza-BODIPY derivatives as NIR probes for cellular imaging. RSC Adv. 2014;4(5):2306-9.

[15] Fan G, Yang L, Chen Z. Water-soluble BODIPY and aza-BODIPY dyes: synthetic progress and applications. Front Chem Sci Eng. 2014;8(4):405-17.

[16] D'Aléo A, Fages F. Boron Complexes as Solid-State Fluorophores. Display Imaging. 2014;1(2):149-74.

[17] Zhao Z, Chen B, Geng J, Chang Z, Aparicio-Ixta L, Nie H, et al. Red Emissive Biocompatible Nanoparticles from Tetraphenylethene-Decorated BODIPY Luminogens for Two-Photon Excited Fluorescence Cellular Imaging and Mouse Brain Blood Vascular Visualization. Part Part Syst Charact. 2014;31(4):481-91.

[18] Gomez-Duran CFA, Hu R, Feng G, Li T, Bu F, Arseneault M, et al. Effect of AIE Substituents on the Fluorescence of Tetraphenylethene-Containing BODIPY Derivatives. ACS Appl Mater Interfaces. 2015;7(28):15168-76.

[19] Zhang G, Chen J, Payne SJ, Kooi SE, Demas JN, Fraser CL. Multi-Emissive Difluoroboron Dibenzoylmethane Polylactide Exhibiting Intense Fluorescence and Oxygen-Sensitive Room-Temperature Phosphorescence. J Am Chem Soc. 2007;129(29):8942-3.

[20] Pfister A, Zhang G, Zareno J, Horwitz AF, Fraser CL. Boron Polylactide Nanoparticles Exhibiting Fluorescence and Phosphorescence in Aqueous Medium. ACS Nano. 2008;2(6):1252-8.

[21] Zhang G, Singer JP, Kooi SE, Evans RE, Thomas EL, Fraser CL. Reversible solid-state mechanochromic fluorescence from a boron lipid dye. J Mater Chem. 2011;21(23):8295-9.

[22] Nguyen ND, Zhang G, Lu J, Sherman AE, Fraser CL. Alkyl chain length effects on solid-state difluoroboron β-diketonate mechanochromic luminescence. J Mater Chem. 2011;21(23):8409-15.

[23] Lanoë P-H, Mettra B, Liao YY, Calin N, D'Aléo A, Namikawa T, et al. Theoretical and Experimental Study on Boron β-Diketonate Complexes with Intense Two-Photon-Induced Fluorescence in Solution and in the Solid State. ChemPhysChem. 2016;17(14):2128-36.

[24] Poon C-T, Wu D, Yam VW-W. Boron(III)-Containing Donor–Acceptor Compound with Goldlike Reflective Behavior for Organic Resistive Memory Devices. Angew Chem Int Ed. 2016;55(11):3647-51.

[25] Domercq B, Grasso C, Maldonado J-L, Halik M, Barlow S, Marder SR, et al. Electron-Transport Properties and Use in Organic Light-Emitting Diodes of a Bis(dioxaborine)fluorene Derivative. J Phys Chem B. 2004;108(25):8647-51.

[26] Hales JM, Matichak J, Barlow S, Ohira S, Yesudas K, Brédas J-L, et al. Design of Polymethine Dyes with Large Third-Order Optical Nonlinearities and Loss Figures of Merit. Science. 2010;327(5972):1485-8.

[27] Karpenko IA, Niko Y, Yakubovskyi VP, Gerasov AO, Bonnet D, Kovtun YP, et al. Push-pull dioxaborine as fluorescent molecular rotor: far-red fluorogenic probe for ligand-receptor interactions. J Mater Chem C. 2016;4(14):3002-9.

[28] Ran C, Xu X, Raymond SB, Ferrara BJ, Neal K, Bacskai BJ, et al. Design, Synthesis, and Testing of Difluoroboron-Derivatized Curcumins as Near-Infrared Probes for in Vivo Detection of Amyloid-β Deposits. J Am Chem Soc. 2009;131(42):15257-61.

[29] Zhang X, Tian Y, Li Z, Tian X, Sun H, Liu H, et al. Design and Synthesis of Curcumin Analogues for in Vivo Fluorescence Imaging and Inhibiting Copper-Induced Cross-Linking of Amyloid Beta Species in Alzheimer's Disease. J Am Chem Soc. 2013;135(44):16397-409.

[30] Felouat A, D'Aléo A, Fages F. Synthesis and Photophysical Properties of Difluoroboron Complexes of Curcuminoid Derivatives Bearing Different Terminal Aromatic Units and a meso-Aryl Ring. J Org Chem. 2013;78(9):4446-55.

[31] D'Aleo A, Felouat A, Heresanu V, Ranguis A, Chaudanson D, Karapetyan A, et al. Two-photon excited fluorescence of BF2 complexes of curcumin analogues: toward NIR-to-NIR fluorescent organic nanoparticles. J Mater Chem C. 2014;2(26):5208-15.

[32] Liu K, Chen J, Chojnacki J, Zhang S. $BF_3 \cdot OEt_2$-promoted concise synthesis of difluoroboron-derivatized curcumins from aldehydes and 2,4-pentanedione. Tetrahedron Lett. 2013;54(16):2070-3.

[33] Bai G, Yu C, Cheng C, Hao E, Wei Y, Mu X, et al. Syntheses and photophysical properties of BF_2 complexes of curcumin analogues. Org Biomol Chem. 2014;12(10):1618-26.

[34] Kim E, Felouat A, Zaborova E, Ribierre J-C, Wu JW, Senatore S, et al. Borondifluoride complexes of hemicurcuminoids as bio-inspired push-pull dyes for bioimaging. Org Biomol Chem. 2016;14:1311-24.

[35] Rivoal M, Zaborova E, Canard G, D'Aléo A, Fages F. Synthesis, electrochemical and photophysical studies of the borondifluoride complex of a meta-linked biscurcuminoid. New J Chem. 2016;40(2):1297-305.

[36] Štefane B. Selective Addition of Organolithium Reagents to BF_2-Chelates of β-Ketoesters. Org Lett. 2010;12(13):2900-3.

[37] Parker CA. Photoluminescence of Solutions. Amsterdam: Elsevier Publishing, 1969.

[38] Lakowicz JR. Principles of Fluorescence Spectroscopy. 3rd ed. New-York (NY): Kluwer, 2006

[39] Crosby GA, Demas JN. Measurement of photoluminescence quantum yields. Review. J Phys Chem. 1971;75(8):991-1024.

[40] Connelly NG, Geiger WE. Chemical Redox Agents for Organometallic Chemistry. Chem Rev. 1996;96(2):877-910.

[41] Frisch MJ, Trucks GW, Schlegel HB, Scuseria GE, Robb MA, Cheeseman JR, et al. Gaussian 09, Revision B.01. Gaussian 09, Revision B01. 2009.

[42] Adamo C, Barone V. Toward reliable density functional methods without adjustable parameters: The PBE0 model. J Chem Phys 1999,;110(13):6158−70.

[43] Ernzerhof M, Scuseria GE. Assessment of the Perdew-Burke-Ernzerhof Exchange-Correlation Functional. J Chem Phys. 1999;110:5029−36.

[44] Tomasi J, Mennucci B, Cammi R. Quantum Mechanical Continuum Solvation Models. Chem Rev. 2005;105(8):2999-3094.

[45] Cossi M, Barone V. Time-dependent density functional theory for molecules in liquid solutions. J Chem Phys. 2001;115:4708−17.

[46] Improta R, Barone V, Scalmani G, Frisch MJ. A state-specific polarizable continuum model time dependent density functional theory method for excited state calculations in solution. J Chem Phys. 2006;125:054103.

[47] Reichardt C. Solvatochromic Dyes as Solvent Polarity Indicators. Chem Rev. 1994;94(8):2319-58.

[48] D'Aléo A, Gachet D, Heresanu V, Giorgi M, Fages F. Efficient NIR-Light Emission from Solid-State Complexes of Boron Difluoride with 2′-Hydroxychalcone Derivatives. Chem Eur J. 2012;18(40):12764-72.

[49] D'Aléo A, Heresanu V, Giorgi M, Le Guennic B, Jacquemin D, Fages F. NIR Emission in Borondifluoride Complexes of 2′-Hydroxychalcone Derivatives Containing an Acetonaphthone Ring. J Phys Chem C. 2014;118(22):11906-18.

[50] Kamada K, Namikawa T, Senatore S, Matthews C, Lenne P-F, Maury O, et al. Borondifluoride Curcuminoid Fluorophores with Enhanced Two-Photon Excited Fluorescence Emission and Versatile Living-Cell Imaging Properties. Chem Eur J. 2016;22(15):5219–32.

[51] Lippert E. Dipolmoment und elektronenstruktur von angeregten molekülen. Naturforsch. 1955;10a:541-5.

[52] Mataga EZ, Kaifu Y, Koizumi M. Solvent Effects upon Fluorescence Spectra and the Dipole-moments of Excited Molecules. Bull Chem Soc Jpn 1956;29:465-70.

[53] Lippert E. Spectroscopic determination of the dipole moment of aromatic compounds in the first excited singlet state. Z Elektrochem. 1957;61:962-75.

[54] Leroy S, Soujanya T, Fages F. Zinc(II)-operated intramolecular charge transfer fluorescence emission in pyrene-2,2′-bipyridine conjugated molecular rods. Tetrahedron Lett. 2001;42(9):1665-7.

[55] Leroy-Lhez S, Allain M, Oberle J, Fages F. Synthesis and zinc(II) complexation modulated fluorescence emission properties of two pyrene-oligo(phenylene vinylene)-2,2'-bipyridine conjugated molecular rods. New J Chem. 2007;31(6):1013-21.

[56] Benniston AC, Grosshenny V, Harriman A, Ziessel R. New J Chem. 1997;21(21):405.

Synthesis of new fluorophores based on hemicurcuminoid boron difluoride.

Photophysical study reveals strong emission of the dyes not containing charge transfer states.

Fluorescence properties of dyes in their condensed phase show aggregation induced emission.